Ba- AND Ti-RICH PRIMARY BIOTITE FROM THE BROME ALKALINE IGNEOUS COMPLEX, MONTEREGIAN HILLS, QUEBEC: MECHANISMS OF SUBSTITUTION
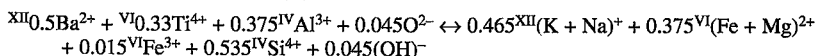
C. MICHAEL B. HENDERSON[1]

Department of Geology, The University, Manchester M13 9PL, U.K.

KENNETH A. FOLAND

Department of Geology, Ohio State University, Columbus, Ohio 43210, U.S.A.

ABSTRACT

An alkaline gabbro from the Brome complex, in Quebec, contains abundant biotite that is highly enriched in Ba and Ti. A bulk-mica sample has been analyzed for structural H_2O, FeO and Fe_2O_3, and by Fe and Ti K-edge and Ti L-edge X-ray absorption spectroscopy to provide information on the valency and coordination states of Fe and Ti. Fe^{3+} makes up a maximum of 10% of total iron, whereas no Ti^{3+} can be detected. There is no spectroscopic evidence suggesting the presence of significant Fe^{3+} or Ti^{4+} in tetrahedral coordination. By combining all this information, it is shown that the bulk biotite contains about 50% of an oxy-mica component ($O^{2-} \leftrightarrow OH^-$) with few or no vacancies in cation sites. Electron-microprobe analyses define core to rim zoning trends of outwardly decreasing Ba, Ti, Al, *mg#* and increasing Si, (Fe + Mn + Mg), (Na + K). The substitution mechanism in the Brome biotite is deduced to be:
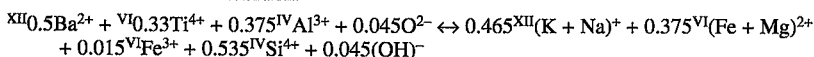
$$^{XII}0.5Ba^{2+} + {}^{VI}0.33Ti^{4+} + 0.375^{IV}Al^{3+} + 0.045O^{2-} \leftrightarrow 0.465^{XII}(K + Na)^+ + 0.375^{VI}(Fe + Mg)^{2+}$$
$$+ 0.015^{VI}Fe^{3+} + 0.535^{IV}Si^{4+} + 0.045(OH)^-$$

Cation-site deficiencies commonly reported for very Ba–Ti-rich biotite in alkaline, basic igneous rocks may be artefacts of using 22-oxygen cell formulae rather than taking account of major replacement of excess O^{2-} for OH^- (oxy-mica substitution).

Keywords: biotite, barium, titanium, substitution mechanism, X-ray absorption spectroscopy, Fe and Ti K and L edge spectroscopy, Brome igneous complex, Quebec.

SOMMAIRE

Un échantillon de gabbro alcalin du complexe igné de Brome, au Québec, contient de la biotite fortement enrichie en Ba et en Ti. Un concentré de biotite a été analysé pour sa teneur en H_2O incorporée dans la structure, en FeO et en Fe_2O_3, et étudiée par spectroscopie de l'absorption X (seuils K et L) pour déterminer la valence et la coordinence du Fe et du Ti. Le Fe^{3+} constitue jusqu'à 10% du fer total, mais nous n'avons pas décelé le Ti^{3+}. Les spectres d'absorption X ne fournissent aucune indication de fractions importantes de Fe^{3+} ou de Ti^{4+} en coordinence tétraédrique. Toute cette information mène aux conclusions que la biotite contient environ 50% d'un composant "oxy-biotite" ($O^{2-} \leftrightarrow OH^-$), et qu'elle est sans lacunes appréciables dans les sites cationiques. Les analyses à la microsonde électronique montrent que la biotite est zonée: la teneur en Ba, Ti et Al et la valeur du *mg#* diminuent vers la bordure des grains, tandis que Si, (Fe + Mn + Mg), et (Na + K) augmentent. Nous en déduisons le mécanisme de substitution:

$$^{XII}0.5Ba^{2+} + {}^{VI}0.33Ti^{4+} + 0.375^{IV}Al^{3+} + 0.045O^{2-} \leftrightarrow 0.465^{XII}(K + Na)^+ + 0.375^{VI}(Fe + Mg)^{2+}$$
$$+ 0.015^{VI}Fe^{3+} + 0.535^{IV}Si^{4+} + 0.045(OH)^-$$

Les lacunes dans les sites cationiques, qui sont couramment attribuées à la biotite enrichie en Ba et en Ti dans les roches ignées basiques et alcalines, pourraient bien être une conséquence de la convention d'écrire la formule avec 22 atomes d'oxygène, sans prendre en considération le présence d'un excès d'oxygène en remplacement partiel du OH (composant "oxy-biotite").

(Traduit par la Rédaction)

Mots-clés: biotite, baryum, titane, mécanisme de substitution, spectroscopie d'absorption X, seuils K et L de Fe et de Ti, complexe igné de Brome, Québec.

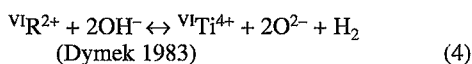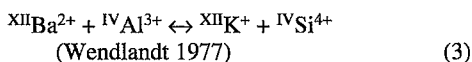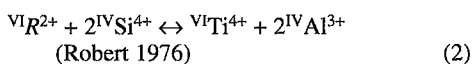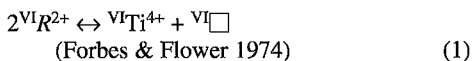[1] *E-mail address:* chenderson@fs2.ge.man.ac.uk

INTRODUCTION

During a geochemical study of subvolcanic alkaline igneous complexes from the Monteregian Hills, Quebec, a sample of alkaline gabbro [locality shown in Foland et al. (1989)] from the gabbro unit in the Brome complex, was found to be particularly rich in a primary, Ba–Ti-rich, red-brown biotite. Similar Ba- and Ti-rich biotite has been reported from ultra-alkaline and alkaline basic igneous rocks, usually as a late-crystallizing, groundmass phase (Wendlandt 1977, Thompson 1977, Mankser et al. 1979, Mitchell & Platt 1984, Edgar 1992, Zhang et al. 1993, Seifert & Kämpf 1994, Shaw & Penczak 1996). More unusually, such compositions are also known from tholeiitic gabbros (Bigi et al. 1993). Although Ba-rich trioctahedral micas occur in high-grade metamorphosed carbonate-rich rocks, they are usually Ti-poor (Solie & Su 1987, Tracy 1991); however, exceptionally Ti- and Ba-rich phlogopite also is known from marble (Bol et al. 1989).

In most of the papers referenced above, the mechanisms of chemical substitution are considered but are generally not well constrained, mainly because the analyses lack H_2O values and information on the oxidation state of Fe (and Ti). In this paper, the substitution mechanisms exhibited by the Ba–Ti-rich biotite from the Brome alkali gabbro will be discussed. Deductions are based on results of electron-microprobe analyses of the zoned grains, combined with $Fe^{2+}:Fe^{3+}$ and H_2O analyses of a bulk-mica separate. In addition, this mica separate was studied using element-specific, X-ray absorption spectroscopic techniques to determine the oxidation state and coordination of Fe and Ti. The compositions of coexisting minerals are also reported and used to deduce the conditions of formation of the mica in order to constrain further the substitution models considered.

MECHANISMS OF Ba AND Ti INCORPORATION IN BIOTITE

Several investigators have considered the substitution mechanisms by which Ba and Ti independently enter biotite:
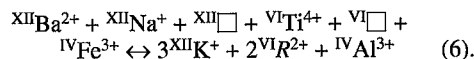
$$2^{VI}R^{2+} \leftrightarrow {}^{VI}Ti^{4+} + {}^{VI}\square$$
(Forbes & Flower 1974)   (1)

$${}^{VI}R^{2+} + 2^{IV}Si^{4+} \leftrightarrow {}^{VI}Ti^{4+} + 2^{IV}Al^{3+}$$
(Robert 1976)   (2)

$${}^{XII}Ba^{2+} + {}^{IV}Al^{3+} \leftrightarrow {}^{XII}K^+ + {}^{IV}Si^{4+}$$
(Wendlandt 1977)   (3)

$${}^{VI}R^{2+} + 2OH^- \leftrightarrow {}^{VI}Ti^{4+} + 2O^{2-} + H_2$$
(Dymek 1983)   (4)

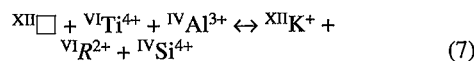leading to the anhydrous end-member "Ti-oxybiotite", $KMg_2TiSi_3AlO_{12}$.

Mankser et al. (1979) suggested that substitutions (1), (2) and (3) occur in biotite from Hawaiian nephelinites and combined them to give the relationship:

$${}^{XII}Ba^{2+} + 2^{VI}Ti^{4+} + {}^{VI}\square + 3^{IV}Al^{3+} \leftrightarrow$$
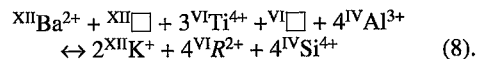$${}^{XII}K^+ + 3^{VI}R^{2+} + 3^{IV}Si^{4+}$$ (5).
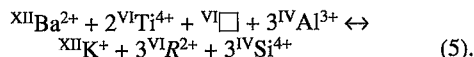
The compositional relations of biotite from West Eifel nephelinites (Edgar 1992) and certain types of lamproites (fitzroyite; Mitchell 1981) seem to be described by equation (5). However, Mitchell (1981) has suggested that other types of lamproite (e.g., wolgidite) show a different trend of substitution that involves entry of Fe^{3+} into tetrahedral sites:

$${}^{XII}Ba^{2+} + {}^{XII}Na^+ + {}^{XII}\square + {}^{VI}Ti^{4+} + {}^{VI}\square +$$
$${}^{IV}Fe^{3+} \leftrightarrow 3^{XII}K^+ + 2^{VI}R^{2+} + {}^{IV}Al^{3+}$$ (6).

An experimental study of Ba partitioning into Ti-rich phlogopite mica led Guo & Green (1990) to modify equation (5) by adding:

$${}^{XII}\square + {}^{VI}Ti^{4+} + {}^{IV}Al^{3+} \leftrightarrow {}^{XII}K^+ +$$
$${}^{VI}R^{2+} + {}^{IV}Si^{4+}$$ (7)

to give:

$${}^{XII}Ba^{2+} + {}^{XII}\square + 3^{VI}Ti^{4+} + {}^{VI}\square + 4^{IV}Al^{3+}$$
$$\leftrightarrow 2^{XII}K^+ + 4^{VI}R^{2+} + 4^{IV}Si^{4+}$$ (8).
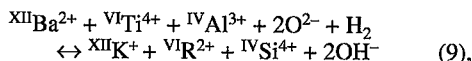
Although all these equations are crystallochemically feasible, their utility in the interpretation of natural biotite trends depends on the completeness of the chemical analysis and on the reliability of the cell-formula calculations. Most authors have relied on electron-microprobe data (i.e., lacking H_2O and, in many cases, halogen data) and recalculated results of analyses to 22 atoms of oxygen assuming that all iron is Fe^{2+}. This basis of calculation assumes the presence of 4 (OH,F,Cl). Thus the presence of excess oxygen due to solid solution of an oxy-mica component $[O^{2-} \leftrightarrow 2OH^-$, equation (4) above] would lead to cation numbers that are too low (cf. Dymek 1983). Under these circumstances, allocation of cations to structural sites can produce unreliable site-totals, perhaps implying the presence of vacancies. By contrast, the presence of Fe^{3+} would lead to cation numbers that are too high if cell-formula calculation is carried out assuming that all iron is present as Fe^{2+} (cf. Dymek 1983).

Many authors have pointed out that cell formulae of Ti-rich and Ba–Ti-rich biotite (22O basis) generally have low tetrahedral cation totals, i.e., Si + Al < 8 (e.g., Wendlandt 1977, Mitchell 1981, Wagner & Velde 1986, Bol et al. 1989, Foley 1989, Zhang et al. 1993,

Seifert & Kämpf 1994). This tetrahedral deficiency is usually assumed to be made up with $^{IV}Fe^{3+}$, as in the end-member mineral "tetraferriphlogopite" (Wendlandt 1977, Arima & Edgar 1981). However, it has also been suggested that Ti enters tetrahedral sites (Carmichael 1967), and Farmer & Boettcher (1981) have predicted that Ti^{4+} should enter 4-fold coordination in preference to Fe^{3+}. The presence of an oxy-mica component would lead to anomalously low cation numbers and thus low (Si + Al) and, therefore, overestimation of $^{IV}Fe^{3+}$ and $^{IV}Ti^{4+}$. Yau et al. (1986) and Bol et al. (1989) have attempted to avoid the underestimation of cation numbers resulting from the presence of the oxy-mica substitution by recalculating cell formulae to a total of 14 tetrahedrally plus octahedrally coordinated cations. Note that this basis of recalculation is strictly only valid in the absence of vacancies in the octahedral or interlayer positions. Seifert & Kämpf (1994) estimated the degree of oxy-mica substitution for an exceptionally F-rich biotite by recalculating cations to 12(O,F) [i.e., 24(O,F), assuming no OH contribution)]. Bol et al. (1989) summarized the oxy-substitution mechanism as follows [equivalent to equations (3) + (4)]:

$$^{XII}Ba^{2+} + {}^{VI}Ti^{4+} + {}^{IV}Al^{3+} + 2O^{2-} + H_2$$
$$\leftrightarrow {}^{XII}K^+ + {}^{VI}R^{2+} + {}^{IV}Si^{4+} + 2OH^- \qquad (9),$$

leading to the hypothetical anhydrous end-member $BaMg_2TiSi_2Al_2O_{12}$.

On the basis of the above discussion, it is clear that in the absence of a complete chemical analysis, the complex stoichiometry of such biotite makes it very difficult to obtain reliable cell formulae.

EXPERIMENTAL METHODS

The chemical compositions of the coexisting minerals in sample 83/59 have been determined in the University of Manchester using a Cameca Camebax microprobe fitted with a Link Systems 860–500 energy-dispersion detector. A 10-μm-diameter beam was used to minimize alkali loss in the biotite. For the biotite, Al, Ti, Ba (Ti and Ba peaks showed no significant overlap), Na and F were determined by wavelength-dispersion analysis, and other elements by energy dispersion (ED); analytical results were calculated to 22 atoms of oxygen and used to plot variation diagrams. ED only was used for the other minerals.

A bulk biotite separate was chemically analyzed for FeO (12.12 wt%) by the ammonium metavanadate method at Manchester University, and for FeO (11.96 wt%) and total Fe as FeO (13.25 wt%) by the dipyridyl method at the Natural History Museum, London. Using the total Fe reported by chemical analysis and the mean of the two FeO determinations yields 1.33% Fe_2O_3 for the biotite separate. The H_2O

content of the biotite, obtained by thermogravimetric methods at SURRC, East Kilbride, is 1.67 wt.%. It was also obtained from the (OH) content estimated from an infrared spectrum using other analyzed micas as standards; this gave a value of 1.8%, in good agreement with the direct determination. The δD value for the biotite separate was kindly determined by Dr. Gawen Jenkin at the Scottish Universities Research Reactor Centre.

Using the same biotite separate, the valencies of Fe and Ti, and the coordinations of the structural sites they occupy, were investigated using X-ray absorption spectroscopy (XAS). In K-edge spectra for the first series of transition elements, pre-edge and edge features are particularly rich in structural information (e.g., Waychunas et al. 1983, Waychunas 1987, Henderson et al. 1993, 1995). Although the structural information at the 3d K-edges is element-specific, if an element occurs in more than one site, an average environment is obtained. K-edge XAS spectra consist of several regions, namely pre-edge, edge and near-edge structure (XANES), which provide information on valency, coordination number, and site symmetry. Pre-edge and edge features are generally associated with electron transitions to localized states (e.g., the pre-edge is due to low-probability 1s–3d transitions), whereas XANES features result from multiple scattering effects; all yield qualitative three-dimensional information. In contrast, data reduction of the Extended X-ray Absorption Fine Structure (EXAFS) gives one-dimensional, radial, short-range (i.e., to about 6 Å) structural information in the form of average bond-lengths, coordination numbers, and Debye–Waller factors (disorder parameters).

For 3d-transition elements, the information contained in L-edge spectra is significantly different from that obtainable from K-edge EXAFS. Thus in L_2 and L_3 spectra, localized state transitions ($2p \rightarrow 3d$) have a high probability and provide information on the oxidation state (including mixed valencies), site symmetry, spin state, and crystal-field splitting (e.g., de Groot et al. 1992, van der Laan et al. 1992, Cressey et al. 1993, Henderson et al. 1995, Schofield et al. 1995). K-edge and L-edge spectra for the biotite and for various compounds of known structure (model compounds) were obtained at the Daresbury Synchrotron Radiation Source (SRS), U.K. Experimental details for K-edges are as given in Henderson et al. (1993), and for L-edges, in Cressey et al. (1993).

RESULTS

Petrography and mineralogy of
Mount Brome alkaline gabbro 83/59

The biotite forms platy crystals up to about 2 mm long, and also occurs interstitially between

euhedral crystals of clinopyroxene (1–2 mm) and plagioclase (up to 4 mm). The plagioclase shows a laminated texture. The rock also contains well-shaped olivine (2 mm), poikilitic brown amphibole up to 8 mm across, and abundant accessory ilmenite, magnetite and apatite (Table 1). Biotite tends to be closely associated with, or partly enclosed by, the opaque oxides, whereas apatite inclusions are common in both biotite and amphibole, but rare in the cumulus phases olivine, augite and plagioclase. Thus textural relations are generally consistent with biotite, amphibole, opaque oxides and apatite being relatively late magmatic phases. The δD ratio for the biotite (–77.8‰) is consistent with a primary magmatic source of H_2O from the upper mantle (Kyser 1986).

Modal and chemical data for the bulk rock are shown in Table 1; note in particular the high TiO_2, BaO and SrO contents. Analyses and cell formulae of representative biotite from Brome are given in Table 2, and of the coexisting minerals in Table 3. The average of 56 microprobe analyses of the biotite (Table 2, column 1) shows that it is unusually depleted in K and Si and enriched in Ba, Al and Ti. Single-spot analyses with the highest and lowest Ba contents also are shown

TABLE 1. MODAL AND CHEMICAL COMPOSITION OF ALKALI GABBRO SAMPLE 83/59, BROME IGNEOUS COMPLEX

Modal analysis (vol. %)		Chemistry (wt.%)		CIPW Norm (wt.%)		
Olivine	2.1	SiO_2	39.65		Or	4.57
Augite	20.2	TiO_2	4.29		Ab	13.58
Amphibole	2.2	Al_2O_3	15.11		An	18.47
Biotite	13.8	Fe_2O_3	3.74		SrF^*	1.30
Plagioclase	52.7	FeO	7.91		BaF^*	7.28
Apatite	3.6	MnO	0.21		Ne	6.90
Fe-oxides	5.4	MgO	7.10		Wo	9.39
		CaO	11.23	Di	En	6.74
		Na_2O	3.11		Fs	1.81
		K_2O	0.77	Ol	Fo	7.67
		P_2O_5	2.26		Fa	2.26
		SrO	0.41		Ap	5.23
		BaO	2.97		Il	8.15
		Ig. Loss	1.73		Mt	5.42
		Total	100.49			98.77
		mg# (atom)	0.563			

* = SrF and BaF are normative equivalents of Sr and Ba as feldspars
mg# = atomic ratio Mg/(total Fe + Mg)

TABLE 2. RESULTS OF ELECTRON–MICROPROBE ANALYSES OF REPRESENTATIVE BIOTITE CRYSTALS FROM BROME, COMPARED WITH COMPOSITION OF Ba–Ti–RICH BIOTITE FROM OTHER LOCALITIES

	1*	1a	2	3	4Core	5Rim	6	7	8	9	10	11	11a
SiO_2	29.87		27.42	32.89	27.32	31.40	24.2	21.1	33.08	31.60	31.23	24.34	
TiO_2	9.06		10.17	8.00	9.73	8.34	14.1	13.1	6.79	13.06	5.28	13.16	
Al_2O_3	16.65		17.28	15.97	17.48	16.35	16.8	17.6	14.97	14.47	15.26	18.87	
Fe_2O_3	1.33												
FeO	11.89		13.74	12.22	13.36	12.30	9.8	13.2	13.72	10.24	15.81	6.07	
MnO	0.07		0.20	0.19	n.d.	n.d.	-	-	0.08	0.09	0.11	n.d.	
MgO	11.91		10.52	14.09	11.16	13.76	11.3	8.1	13.71	11.82	18.28	11.98	
CaO	0.02		n.d.	n.d.	n.d.	n.d.	0.23	0.21	0.51	0.13	0.22	-	
BaO	12.65		16.06	8.39	15.90	10.44	14.5	20.5	9.76	10.91	15.21	24.67	
Na_2O	1.02		0.79	1.14	0.82	0.97	0.57	0.28	n.d.	1.01	0.28	0.58	
K_2O	4.12		3.11	5.41	3.09	4.79	4.3	2.3	5.10	5.18	4.39	1.34	
F	0.24		0.28	0.29	0.28	0.29	-	-	3.44	-	5.41	-	
Cl	0.05		0.01	0.05	0.06	-	-	-	-	-	-	-	
H_2O	1.67												
Total	100.44		99.45	98.50	99.06	98.50	95.8	96.3	98.81	98.51	99.20	100.96	

	24(an)	22(O)	22(O)	22(O)	22(O)	22(O)	22(O)	22(O)	22(O)	22(O)	24(O,F)	22(O)	14cats
Si	4.888	4.672	4.589	5.197	4.597	5.035	3.984	3.677	4.954	4.849	5.082	3.942	4.291
Al	3.112	3.069	3.409	2.803	3.403	2.965	3.260	3.619	2.536	2.617	2.916	3.603	3.709
Total Z	8.000	7.741	7.998	8.000	8.000	8.000	7.244	7.296	7.490	7.466	7.998	7.545	8.000
Al	0.099	-	-	0.171	0.050	0.126	-	-	-	-	-	-	0.213
Ti	1.115	1.066	1.280	0.951	1.225	1.006	1.744	1.722	0.768	1.507	0.646	1.603	1.745
Fe^{3+}	0.163	0.156	1.923	1.615	1.873	1.650	1.353	1.925	1.714	1.314	0.792	0.822	0.895
Fe^{2+}	1.627	1.555											
Mn	0.010	0.009	0.028	0.025	-	-	-	-	0.010	0.012	0.016	-	-
Mg	2.906	2.777	2.624	3.318	2.788	3.289	2.780	2.103	3.060	2.704	4.436	2.892	3.147
Total Y	5.920	5.563	5.855	6.080	5.936	6.071	5.877	5.750	5.552	5.537	5.890	5.317	6.000
Ca	0.004	0.004	-	-	-	-	0.041	0.039	0.082	0.021	0.038	-	-
Ba	0.811	0.775	1.053	0.520	1.044	0.656	0.937	1.402	0.573	0.656	0.970	1.562	1.701
Na	0.325	0.310	0.257	0.351	0.267	0.302	0.182	0.095	-	0.300	0.088	0.182	0.198
K	0.859	0.821	0.665	1.091	0.660	0.979	0.906	0.517	0.974	1.014	0.912	0.277	0.301
Total X	1.999	1.910	1.975	1.962	1.971	1.937	2.066	2.053	1.629	1.991	2.008	2.021	2.200
F	0.124	-	0.149	0.147	0.149	0.149			1.629		2.786		
Cl	0.014	-	0.001	0.013	0.018	-							
OH	1.825	-											
O	22.037	-											
mg#	0.619		0.577	0.673	0.598	0.666	0.673	0.522	0.641	0.673	0.849	0.643	

* Compositions quoted in wt%; sulfur generally <0.1 wt%; n.d. not detected; – not analyzed for; mg# = atomic ratio: Mg/(total Fe + Mg). Columns: (1–5) Brome gabbro, (1) Average of 56 analyses, formula calculated to 24 (O,OH,F,Cl), compare with column (1a) formula to 22(O); (2–5) single spot analyses; (4,5) same grain. (6,7) Mansker et al. (1979; samples 48–80, 48–112); (8) Edgar (1992; sample E3); (9) Zhang et al. (1993; DZ2n); (10) Seifert & Kämpf (1994; KB average of 42 analyses); (11) Bol et al. (1989; B046), formulae calculated to 22(O) and (11a) Z + Y = 14 cations.

TABLE 3. REPRESENTATIVE COMPOSITIONS OF MINERALS COEXISTING WITH BIOTITE IN ALKALI GABBRO FROM THE BROME COMPLEX

	1* (4)	2 (11)	3 (4)	4 (5)	5 (8)	6	7	8 (3)
SiO_2	37.69	51.43	41.69	0.32	0.45	55.57	59.83	0.20
TiO_2	-	1.29	5.38	48.20	6.50	-	-	-
Al_2O_3	-	2.94	11.52	0.21	3.34	27.44	24.77	-
Cr_2O_3	-	0.05	0.08	0.07	0.12	-	-	-
FeO	29.36	7.18	11.40	47.99	82.07	0.12	0.50	0.29
MnO	0.82	0.24	0.22	1.30	0.28	-	-	n.d.
MgO	33.33	14.26	12.87	0.98	0.66	-	-	n.d.
CaO	0.05	22.01	11.64	0.03	0.07	9.29	5.75	54.8
Na_2O	-	0.49	2.99	-	-	5.99	7.69	0.05
K_2O	-	-	0.64	-	-	0.04	0.27	n.d.
SrO	-	-	-	-	-	1.06	-	0.49
BaO	-	-	0.50	-	-	0.80	0.21	n.d.
P_2O_5	-	-	-	-	-	-	-	40.58
F	-	-	0.25	-	-	-	-	2.62
Cl	-	-	0.02	-	-	-	-	0.20
Total	101.24	99.89	99.09	99.10	93.49	100.31	99.02	98.13
	4(O)	6(O) 4(Cat)$	23(O)	24(O) 16(Cat)	32(O) 24(Cat)	8(O)	8(O)	25(O)
Si	1.003	1.907	6.115	0.063	0.135	2.517	2.676	0.034
Al		0.129	1.992	0.051	1.191	1.465	1.306	
Ti		0.036	0.593	7.286	1.478			
Cr			0.009	0.011	0.029			
Fe^{3+}		0.021		1.238	11.553	0.004	0.019	
Fe^{2+}	0.653	0.212	1.398	6.829	9.222			0.042
Mn	0.018	0.007	0.027	0.221	0.072			
Mg	1.321	0.788	2.813	0.293	0.296			
Ca	0.002	0.874	1.829	0.007	0.024	0.451	0.276	10.065
Na		0.035	0.849			0.526	0.667	0.016
K			0.120			0.002	0.015	
Sr						0.028		0.048
Ba			0.029			0.014	0.004	
P								5.887
F			0.116					1.420
Cl			0.005					0.057
$mg\#$	0.665	0.774	0.664	0.034	0.014	An% 46.1	28.6	

* Minerals (average result of the number of analyses given in parentheses): 1 olivine, 2 augite, 3 amphibole, 4 ilmenite, 5 magnetite, 6,7 plagioclase, 8 apatite. $: recalculated to standard number of cations to obtain Fe oxidation ratio.

The compositions of coexisting olivine, clinopyroxene, amphibole, ilmenite and magnetite all show only limited variation in Mg and Fe compared to the biotite (Fig. 1b). Clinopyroxene has the highest $mg\#$ of the coexisting mafic minerals, whereas olivine and amphibole have $mg\#$ values similar to those of the most magnesian biotite. The amphibole is Ti-rich (kaersutite) and also is relatively rich in Ba compared to other examples of kaersutite from alkaline basic rocks (Henderson & Gibb 1987). Both Fe-oxide phases are essentially homogeneous on a 5 µm scale. The coexisting plagioclase is comparatively rich in Ba and shows limited Ca ↔ Na zoning (Fig. 1a). In comparison to other differentiated alkaline basaltic intrusions, the An contents are rather low considering the $mg\#$ values of the coexisting mafic silicates (Parsons 1981, Wilson & Larsen 1985, Henderson & Gibb 1987, Wadsworth 1988, Gibb & Henderson 1996). Coexisting ilmenite and magnetite compositions give temperature and oxygen fugacities in the ranges 680°–710°C and 10^{-16}–10^{-17} atm., respectively (Powell & Powell 1974). These estimates indicate conditions slightly more oxidizing than the quartz – fayalite – magnetite buffer, in common with some other alkaline igneous rock series (e.g., Parsons et al. 1986, Henderson & Gibb 1987, Henderson et al. 1989). The high Ti and Ba contents in the biotite are consistent with crystallization under conditions of high temperature and low pressure (Edgar et al. 1976, Robert 1976, Trønnes et al. 1985, Guo & Green 1990).

In sum, the assemblage of silicate minerals is typical of magmatic conditions of formation for an alkaline basaltic parental magma. However, the temperatures estimated for the Fe-oxides represent conditions of subsolidus re-equilibration. The mineral assemblage crystallized close to the QFM buffer, i.e. under fairly oxidizing conditions. It has not been possible to estimate fugacities for other volatile species, although the F- and Cl-contents of amphibole and biotite (Tables 2, 3) indicate that halogen fugacities were rather low.
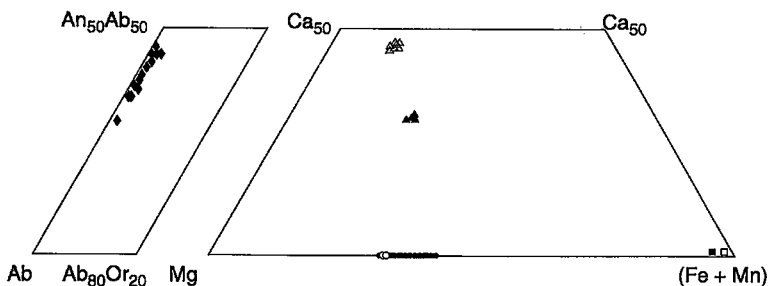
in Table 2 (columns 2 and 3). Biotite cores are clearly more Ba- and Ti-rich than rims (Table 2, columns 4 and 5) and, unusually, these cores have higher Fe/Mg ratios than the rims.

FIG. 1. Compositions of coexisting minerals in Brome gabbro 83/59 (atomic proportions): (a) plagioclase; (b) mafic minerals. Symbols: plagioclase ♦; olivine ○; augite △; kaersutite ▲; biotite ●; magnetite □; ilmenite ■.

Crystal chemistry of the biotite

Pre-edge and XANES features in the Fe and Ti *K*-edge spectra for the Brome biotite and representative model compounds are displayed in Figures 2 and 4, respectively, and for Ti *L*-edge spectra in Figure 3. Refined *K*-edge EXAFS parameters and certain edge data for Fe and Ti are given in Table 4.

The features characteristic of Fe^{2+} and Fe^{3+} in tetrahedral and octahedral coordination are clear (Fig. 2). For both oxidation states, the pre-edge peak at about 7110 eV is larger for tetrahedral than octahedral coordination (Table 4). Pre-edge intensities are larger for 3*d* elements in distorted- than in symmetrical-octahedral coordination. The pre-edge peaks are more intense for Fe^{3+} than for Fe^{2+} because the former has one more *d*-hole, and thus a higher probability of transition than the latter. The very small pre-edge peak of the biotite suggests that Fe is predominantly Fe^{2+} in a symmetrical octahedral environment. Figure 2 also shows that both Fe oxidation states have more pronounced edge-crest features (at about 7120 eV) for 6-fold than for 4-fold coordination. The positions of double-peak XANES features at 7118 and 7120 eV and the pronounced trough at 7130 eV for biotite are very similar to those for hedenbergite, consistent with the bulk of Fe being octahedral Fe^{2+}. Refined bond-lengths

FIG. 3. *L*-edge absorption spectra Ti: L_3 456–460 eV, and L_2 461–465 eV. Model compounds: (a) Vuonnemite, six-coordinated Ti^{3+} at 457 and 461 eV, and $^{VI}Ti^{4+}$ at 456 and 459 eV (Schofield *et al.*, in prep.), (b) $CsAlTiO_4$, $^{IV}Ti^{4+}$, (c) rutile, distorted $^{VI}Ti^{4+}$, (d) benitoite, relatively symmetrical $^{VI}Ti^{4+}$, and (e) biotite from Brome gabbro 83/59.
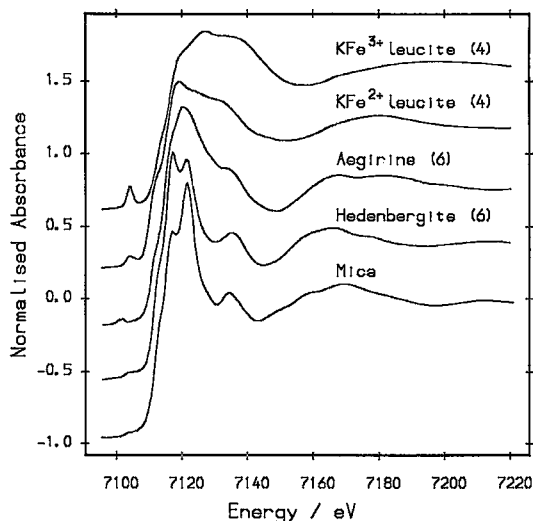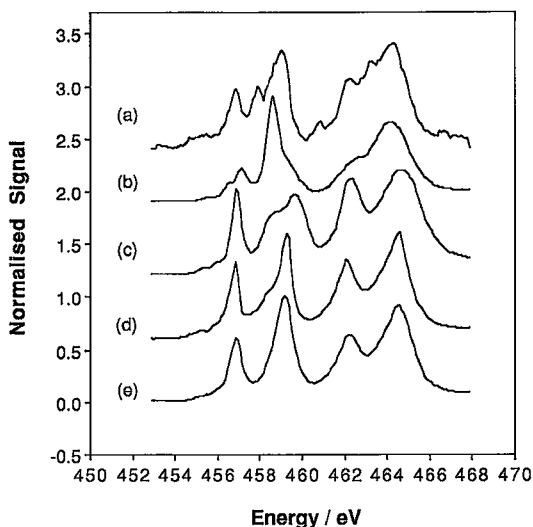

FIG. 2. *K*-edge XANES spectra for Fe in model compounds and in biotite from Brome gabbro 83/59. Model compounds for Fe in 4-coordination: $KFe^{3+}Si_2O_6$ leucite and $K_2Fe^{2+}Si_5O_{12}$ leucite, and for Fe in 6-coordination: $NaFe^{3+}Si_2O_6$ pyroxene (aegirine) and $CaFe^{2+}Si_2O_6$ pyroxene (hedenbergite). The biotite spectrum is consistent with Fe being mainly divalent in octahedral coordination.
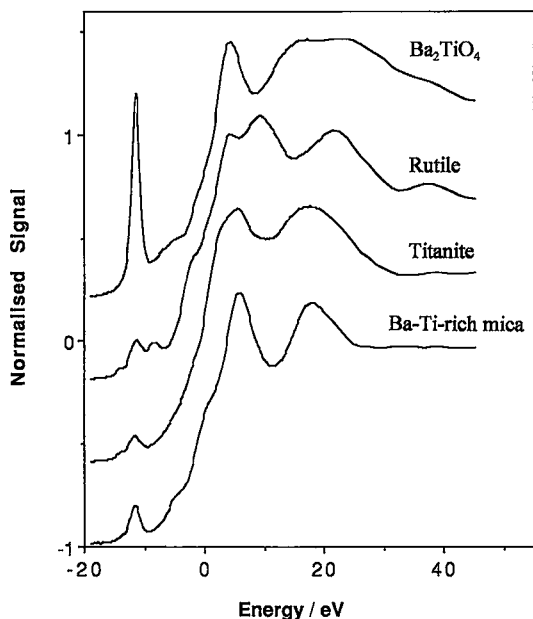
FIG. 4. *K*-edge absorption spectra for Ti in model compounds: Ba_2TiO_4, $^{IV}Ti^{4+}$; rutile, $^{VI}Ti^{4+}$; titanite, $^{VI}Ti^{4+}$, and in biotite from Brome gabbro 83/59. The biotite spectrum shows that Ti is dominantly tetravalent in octahedral coordination.

TABLE 4. FIRST–SHELL EXAFS AND NEAR–EDGE DATA
FOR Fe AND Ti IN BIOTITE 83/59, BROME IGNEOUS COMPLEX

	N	R(Å)	DW(Å^2)	Pre-edge
Fe^{2+}				
Hedenbergite	6	2.10	0.016	0.02
K-Fe^{2+}-leucite$^{\$}$	4	1.97	0.014	0.05
Fe^{3+}				
Aegirine	6	1.98	0.021	0.02
K-Fe^{3+}-leucite$^{\#}$	4	1.85	0.008	0.12
Biotite (83/59)	5.0	2.09	0.018	0.01
Ti				
Rutile	6	1.93	0.019	0.17
Titanite	1	1.74	0.007	0.12
	5	1.97	0.012	
Benitoite	6	1.91	0.011	0.04
Ba$_2$TiO$_4$	4	1.82	0.006	0.95
Biotite (83/59)	*	1.96	*	0.13

N = Coordination number; R = Distance to first shell of oxygen atoms;
  DW = Debye–Waller factor; Pre-edge = height of pre-edge peak
  relative to edge-step height.
$ = K$_2$Fe^{2+}Si$_5$O$_{12}$; # = KFe^{3+}Si$_2$O$_6$.
* Biotite parameters refined from EXFAS data except that the proximity
  of the Ba-L$_{III}$ edge to the Ti K-edge prevented determination of
  meaningful N fand DW data for Ti. Errors: R 0.02Å; N and DW 20%.

(R, Å) and Debye–Waller factors (D.W., Å^2) for the first coordination shell of nearest-neighbor atoms of oxygen in model compounds define "standard" values for both oxidation states in tetrahedral and octahedral coordination R, (D.W.): ^{VI}Fe^{2+}: 2.12, (0.02); ^{IV}Fe^{2+} 1.98,(0.015); ^{VI}Fe^{3+} 2.02, (0.015); ^{IV}Fe^{3+} 1.86, (0.008). As expected, Fe–O distances are larger for Fe^{2+} than for Fe^{3+} and for 6- compared to 4-fold coordination. Debye–Waller factors for Fe^{3+} in tetrahedral coordination are much smaller than for octahedral coordination, resulting from the decreased static disorder around the metal sites in the former. The Debye–Waller factors for Fe^{2+} in tetrahedral coordination are only slightly smaller than for octahedral coordination, suggesting that the larger Fe^{2+} forms significantly less regular 4-fold complexes than the smaller Fe^{3+}. The refined EXAFS parameters for the biotite are closely similar to those for hedenbergite, confirming the suggestion that Fe in the biotite is mainly octahedral Fe^{2+}.

The bulk atomic Fe^{2+}:Fe^{3+} ratio for the Brome biotite shows the presence of about 9% of total Fe as Fe^{3+} but, because Fe^{3+} is subordinate, the EXAFS data cannot be used to reliably deduce whether it is 4- or 6-coordinated. The pre-edge peak in the biotite (0.01 relative to the height of the edge step) is smaller than that for the model compounds studied with ^{VI}Fe^{2+} [e.g., the pre-edge peak heights in hedenbergite and fayalite

both have values of 0.02: Henderson et al. (1995)], showing that the bulk of the Fe in the biotite is in a particularly undistorted site. Although it is impossible to be categorical, the small pre-edge in the biotite suggests that minimal ^{IV}Fe^{3+} is present, as this species has a pre-edge peak height of 0.12 (Table 4). If it is assumed that all the Fe^{3+} in the biotite is in tetrahedral coordination, its contribution to the pre-edge would be 0.011, which would lead to an overall peak-height greater than 0.02, in contrast to the value of 0.01 observed.

The coexisting Fe–Ti oxides show that the mineral assemblage crystallized under conditions slightly more oxidizing that the QFM buffer, suggesting that all Ti should be present as Ti^{4+}. The L-edge spectrum of the rare mineral vuonnemite, which has a substantial amount of total Ti as Ti^{3+} (Ercit & Hawthorne 1987), shows characteristic peaks at about 457 and 460 eV, which are almost certainly due to Ti^{3+}. The lack of Ti^{3+} in the Brome biotite is confirmed by the total absence of peaks at these energies (Fig. 3). The L-edge spectrum for the biotite is similar to that of the model compound benitoite (Fig. 3), and the K-edge spectra for Ti shows pre-edge and XANES features similar to those for titanite (Fig. 4), suggesting that the bulk of Ti is present as ^{VI}Ti^{4+}. From the refined EXAFS data, the first shell Ti–O distance for the biotite (Table 4) is characteristic of that for Ti^{4+} in octahedral coordination; on the basis of values for the Ti–O bond-length and pre-edge height, not more than 10% of the Ti can be in tetrahedral sites (cf. Ryabchikov et al. 1981).

An estimate of the bulk chemical composition of the biotite was obtained by averaging results of 56 microprobe analyses. This method gives a mean total Fe as FeO content of 13.08 wt%, in excellent agreement with the chemical determination of 13.25 wt%. The analyzed Fe^{2+}/Fe^{3+} value was used to obtain FeO and Fe$_2$O$_3$ contents for the average microprobe-derived composition. Table 2, column 1 gives the average microprobe data, together with the directly determined H$_2$O content, and with the cell formula calculated to 24(O, OH, F, Cl). This basis for recalculation gives (Si + Al) slightly in excess of 8.0 [^{VI}Al 0.10 atoms per formula unit, apfu), and very small proportions of vacancies in octahedral and interlayer positions (1.3% and 0.05%, respectively). From these data, there appear to be effectively no vacancies in the interlayer site and a very small proportion of octahedral vacancies. Thus, within analytical error, mechanisms of substitution involving reactions (1) and (5) seem to be limited in extent, whereas those involving reactions (6) and (8) are not valid, for the average composition at least. Note also that the oxy-mica substitution makes up 51% of the "OH" site. By contrast, calculation to 22(O), the conventional basis, gives significantly reduced cation numbers: (Si + Al) (2.9% vacant), octahedral (7.3% vacant) and interlayer (4.9% vacant).

DISCUSSION

Mechanisms of element substitution in biotite

The full range of zoning is exhibited for the individual microprobe analyses in Figure 5, plotted against Ba. Note that the cell-formula data plotted are based on 22 atoms of oxygen. As discussed above,

the presence of "excess" oxygen in the average composition of the Brome mica suggests that these cation numbers are underestimates and could be increased to more realistic values by normalizing to a fixed number of cations (*e.g.*, assuming that interlayer sites are full). However, such a procedure would not change the slopes of the trends, and would only move all data points by a fixed proportion; thus we have
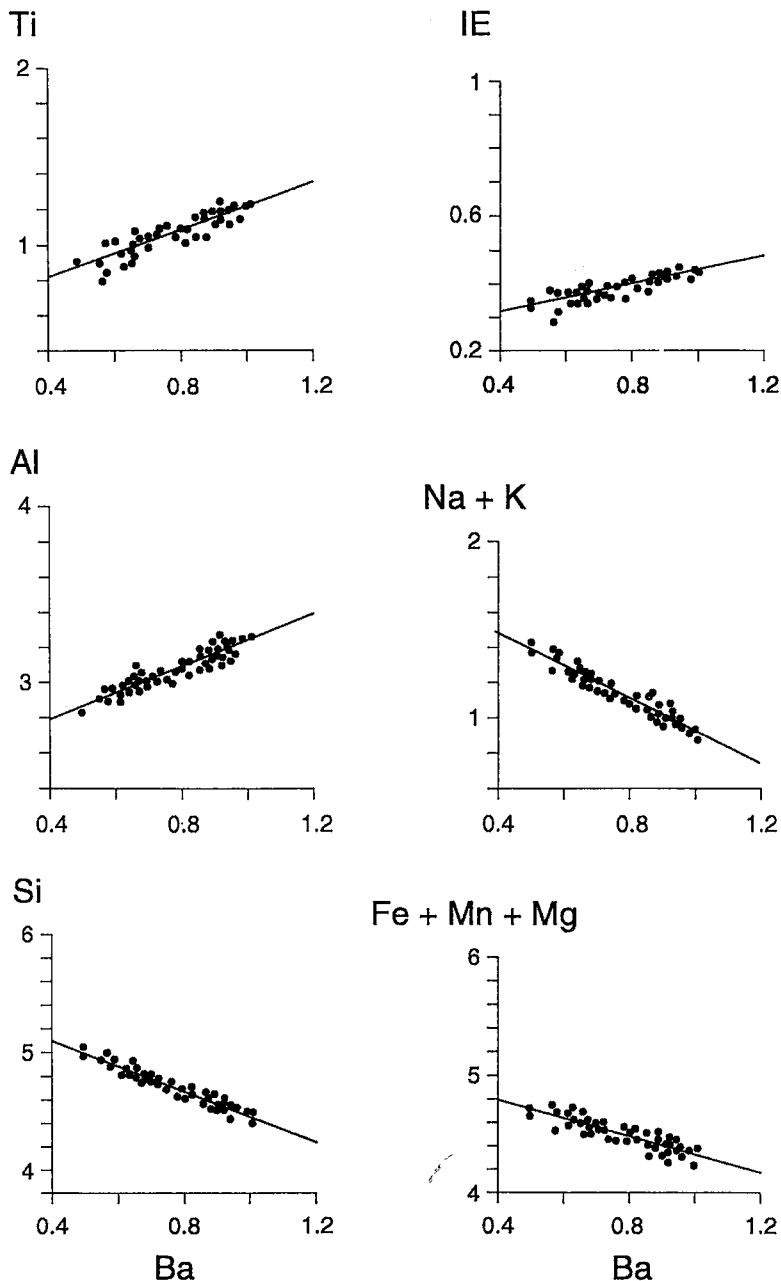

FIG. 5. Zoning trends for biotite in Brome gabbro 83/59 plotted *versus* Ba content. Data plotted are cations per 22(O); I.E., iron enrichment index (Fe + Mn):(Fe + Mn + Mg). Regression lines shown are those defined in Table 5.
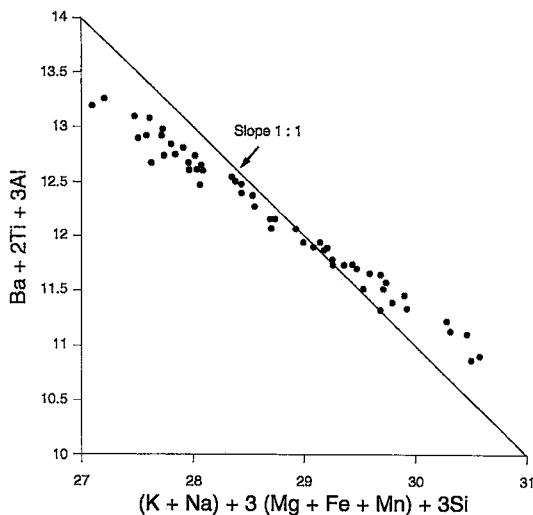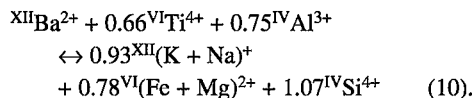
FIG. 6. Zoning trend of Brome biotite plotted as Ba + 2Ti + 3Al versus K + 3(R^{2+}) + 3Si. Note that the slope (−0.69) is significantly less than that of the 1:1 line (substitution mechanism 5).

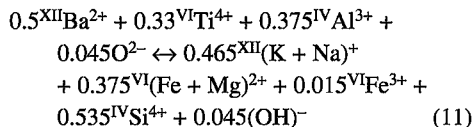chosen to plot the "raw" data. The scatter of points in Figure 5 is generally at or within the level of 2σ analytical error.

Ba is seen to be positively correlated with Al and Ti and negatively correlated with Si, (Mg + Mn + Fe) and (Na + K). These trends have the same form as those reported for other examples of Ba–Ti-rich biotite (Edgar 1992, Zhang *et al.* 1993, Seifert & Kämpf 1994). In addition, for the Brome sample, the Ba is positively correlated with the iron enrichment (I.E.) index (Fe + Mn)/(Fe + Mn + Mg). This last relationship is also evident in the trends illustrated by Mankser *et al.* (1979) and Wendlandt (1977).

Mankser *et al.* (1979) attributed the exchange mechanism in Hawaiian Ba–Ti-enriched biotite to equation (5) on the basis of data showing a 1:1 slope in a Ba + 2Ti + 3Al *versus* K + 3(Mg,Fe) + 3Si plot. Mitchell (1981), Edgar (1992) and Seifert & Kämpf (1994) also have demonstrated good trends on this type of variation diagram, but the plots generally depart

TABLE 5. REDUCED LINEAR MAJOR AXIS REGRESSION FOR BIOTITE 83/59, BROME IGNEOUS COMPLEX

y	x	m	c	R^2
Si	Ba	-1.07	5.52	-0.96
Al	Ba	0.76	2.49	0.93
Ti	Ba	0.66	0.55	0.88
Fe+Mn+Mg	Ba	-0.78	5.11	-0.88
Na+K	Ba	-0.93	1.85	-0.96
I.E.*	Ba	0.20	0.22	0.44

Regression of data shown in Figure 3. m = slope y/x; c = intercept on y; R^2 = regression coefficient. I.E.: atomic (total Fe + Mn)/(total Fe + Mn + Mg)

from a 1:1 slope; the data for the Brome biotite define a similar trend (Fig. 6) of slope −0.69. Thus a more complex scheme of substitution than that defined by equation (5) is indicated. To establish the actual trend for the biotite from Brome, the positive correlations for Ba *versus* Ti and Al and negative correlations for Ba *versus* (Na + K), (Fe + Mg) and Si have been fitted by linear regression; the regression parameters and correlation coefficients are reported in Table 5. The substitution equation obtained has the form:

$$^{XII}Ba^{2+} + 0.66^{VI}Ti^{4+} + 0.75^{IV}Al^{3+}$$
$$\leftrightarrow 0.93^{XII}(K + Na)^+$$
$$+ 0.78^{VI}(Fe + Mg)^{2+} + 1.07^{IV}Si^{4+} \quad (10).$$

This equation does not quite balance; there is a positive excess in charges of 0.12 on the left-hand side. The range of compositional zoning shown in the sample is equivalent to a change of about 0.5 Ba *apfu*, and the actual substitution observed would therefore have a charge excess of 0.06 on the left-hand side. There is no possibility of significant Ti^{3+} occurring for a mineral assemblage buffered by the QFM buffer, and indeed none was detected by XAS. However, the charge excess will be further reduced if a fraction of the Fe component in 6-coordination consists of Fe^{3+}. Thus, if it is assumed that the Fe^{3+}:total Fe ratio is the same as in the bulk sample (0.10), the charge excess would be reduced to only 0.045. This value could be within error, but it is likely that an oxy-mica component should be added, giving the overall substitution:

$$0.5^{XII}Ba^{2+} + 0.33^{VI}Ti^{4+} + 0.375^{IV}Al^{3+} +$$
$$0.045O^{2-} \leftrightarrow 0.465^{XII}(K + Na)^+$$
$$+ 0.375^{VI}(Fe + Mg)^{2+} + 0.015^{VI}Fe^{3+} +$$
$$0.535^{IV}Si^{4+} + 0.045(OH)^- \quad (11)$$

The coefficients in equation (11) imply that the occupancies for each of the sites vary as a result of this mechanism of substitution, but such variations are very small in comparison to the total site-occupancies and might be within error of the method used to characterize the substitution. Thus, as a result of reaction (11), the Ba-rich compositions (left-hand side) are associated with apparent increases in the proportions of vacancies of 2% for (IV)-fold and 1.2% for (VI)-fold sites, whereas the relatively alkali-rich compositions (right-hand side) suggest a vacancy increase of 1.8% in the interlayer site.

The details of this substitution mechanism are likely to be unique to the Brome sample, but it is possible that the general relations are transferable to other occurrences. In particular, it seems likely that the cation-site deficiencies commonly reported for very Ba–Ti-rich biotite in alkaline, basic igneous rocks may be artefacts of using 22(O)-based cell formulae rather than taking account of major replacement of excess O^{2-} for OH^- (*i.e.*, the oxy-mica substitution).

Petrological considerations

Ba–Ti-rich biotite occurring in alkaline igneous rocks is usually interpreted as being late-magmatic in origin (Mankser *et al.* 1979, Zhang *et al.* 1993, Seifert & Kämpf 1994). Within-grain chemical variations are common, but in general, no regular zoning is detectable (Zhang *et al.* 1993, Seifert & Kämpf 1994). This is presumably due to the tendency of the biotite to occur as a groundmass phase. However, the Brome biotite commonly forms well-shaped crystals, with a core enriched, and rim depleted, in Ba and Ti, pointing to the progressive depletion of these components in the most evolved compositions of magma. Such a relationship is in line with the experimental studies, which suggest that higher Ti contents in the biotite are consistent with crystallization under conditions of higher temperature (and lower pressure) (Edgar *et al.* 1976, Robert 1976, Trønnes *et al.* 1985). Interestingly, Guo & Green (1990) have shown that high Ba contents in phlogopite are favored by low pressure, and the occurrence of Ba–Ti-rich biotite in the groundmass of lavas and in the Brome subvolcanic intrusion is consistent with this observation. Note that Guo & Green (1990) suggested that the concentration of Ba in the higher-temperature biotite is controlled by the high Ti content of such phases *via* a coupled substitution.

It has also been suggested that high Ti in biotite is favored by high $f(O_2)$ (Ryabchikov & Green 1978, Arima & Edgar 1981), whereas Foley (1989) has shown that high Ba is favored by increasing H_2O/CH_4 and $f(O_2)$ and that high Ti is correlated with increasing CO_2/H_2O. The Brome biotite crystallized under conditions slightly more oxidizing than QFM, but this does not necessarily imply high $f(H_2O)$, as indicated by the relatively low content of structural OH⁻ and high oxy-biotite component (51%) in the Brome biotite. Note also the low activity of F and Cl in the Brome biotite (Table 2). The unusually low An contents of plagioclase in Brome alkali gabbro 83/59, compared with the degree of evolution shown by contemporaneous mafic phases (olivine and augite), could be related to the relatively low activity of H_2O. This in turn would lead to displacement of the plagioclase solidus toward more sodic compositions at a given temperature [*i.e.*, not depressed by a high $f(H_2O)$]. It is possible, therefore, that the Brome Ba–Ti-rich biotite formed at relatively high temperature and high oxygen fugacity, and low total pressure, low $f(H_2O)$, and perhaps relatively high $f(CO_2)$. More generally, the fact that most examples of Ba–Ti-rich biotite reported in the literature have low cation numbers, if calculated on a 22(O) basis, might indicate that the conditions leading to a high oxy-mica component are also those that lead to very high Ti (*cf.* Ryabchikov *et al.* 1981) and coupled Ba contents.

We have shown that the biotite zoning is anomalous in that the *mg#* value for the core is smaller than that for the rim (Table 2). It is possible to speculate that this relationship is due to the later stages of biotite crystallization occurring alongside the formation of abundant magnetite, which strongly depleted the liquid in Fe and effectively raised the *mg#* of the magma. It is also interesting to speculate on the Ba content of the magma that crystallized the Brome biotite. Guo & Green (1990) found that the crystal/melt distribution coefficient for biotite (D_{Ba}) decreased with increasing pressure from 10 to 20 kbars, and was less than 1 under all experimental conditions studied. Using phenocryst/ groundmass analytical data, Lemarchand *et al.* (1987) reported biotite D_{Ba} values ranging from 5 to 30, whereas Foley *et al.* (1996) have recently reported a value of 3.5. It is clear that the Brome biotite, with up to 14.3% Ba (16% BaO, Table 2) must have crystallized from a melt having much smaller Ba contents, implying very high D_{Ba} values, close to the upper end of the range reported by Lemarchand *et al.* (1987). Based on the discussion above, it seems likely that Ba distribution coefficient in biotite will be very dependent on composition (and melt structure), with magmas crystallizing at the lowest total pressures, and the highest $f(O_2)$ and $f(CO_2)$, having the highest D_{Ba} values, and leading to very high Ba (and Ti) contents in the biotite.

REFERENCES

ARIMA, M. & EDGAR, A.D. (1981): Substitution mechanisms and solubility of titanium in phlogopites from rocks of probable mantle origin. *Contrib. Mineral. Petrol.* **77**, 288-295.

BIGI, S., BRIGATTI, M.F., MAZZUCCHELLI, M. & RIVALENTI, G. (1993): Crystal chemical variations in Ba-rich biotites from gabbro rocks of lower crust (Ivrea Zone, NW Italy). *Contrib. Mineral. Petrol.* **113**, 87-99.

BOL, L.C.G.M., BOS, A., SAUTER, P.C.C. & JANSEN, J.B.H. (1989): Barium-titanium-rich phlogopites in marbles from Rogaland, southwest Norway. *Am. Mineral.* **74**, 439-447.

CARMICHAEL, I.S.E. (1967): The mineralogy and petrology of the volcanic rocks of the Leucite Hills, Wyoming. *Contrib. Mineral. Petrol.* **15**, 24-66.

CRESSEY, G., HENDERSON, C.M.B. & VAN DER LAAN, G. (1993): Use of L-edge X-ray absorption spectroscopy to characterize multiple valence states of 3d transition elements; a new probe for mineralogical and geochemical research. *Phys. Chem. Minerals* **20**, 111-119.

DYMEK, R.F. (1983): Titanium, aluminum and interlayer substitutions in biotite from high-grade gneisses, West Greenland. *Am. Mineral.* **68**, 880-899.

EDGAR, A.D. (1992): Barium-rich phlogopite and biotite from some Quaternary alkali mafic lavas, West Eifel, Germany. *Eur. J. Mineral.* **4**, 321-330.

————, GREEN, D.H. & HIBBERSON, W.O. (1976): Experimental petrology of a highly potassic magma. *J. Petrol.* **17**, 339-356.

ERCIT, T.S. & HAWTHORNE, F.C. (1987): The crystal structure of vuonnemite, a Ti^{3+} bearing phosphate–silicate mineral. *Geol. Assoc. Can. – Mineral. Assoc. Can., Program Abstr.* **12**, 41.

FARMER, G.L. & BOETTCHER, A.L. (1981): Petrologic and crystal-chemical significance of some deep-seated phlogopites. *Am. Mineral.* **66**, 1154-1163.

FOLAND, K.A., CHEN, JAING-FENG, LINDER, J.S., HENDERSON, C.M.B. & WHILLANS, I.M. (1989): High-resolution $^{40}Ar/^{39}Ar$ chronology of multiple intrusion igneous complexes: application to the Cretaceous Mount Brome complex, Quebec, Canada. *Contrib. Mineral. Petrol.* **102**, 127-137.

FOLEY, S.F. (1989): Experimental constraints on phlogopite chemistry in lamproites. 1. The effect of water activity and oxygen activity. *Eur. J. Mineral.* **1**, 411-426.

————, JACKSON, S.E., FRYER, B.J., GREENOUGH, J.D. & JENNER, G.A. (1996): Trace element partition coefficients for clinopyroxene and phlogopite in an alkaline lamprophyre from Newfoundland by LAM–ICP–MS. *Geochim. Cosmochim. Acta* **60**, 629-638.

FORBES, W.C. & FLOWER, M.F.J. (1974): Phase relations of titan-phlogopite, $K_2Mg_4TiAl_2Si_6O_{20}(OH)_4$: a refractory phase in the upper mantle. *Earth Planet. Sci. Lett.* **22**, 60-66.

GIBB, F.G.F. & HENDERSON, C.M.B. (1996): The Shiant Isles main sill: structure and mineral fractionation trends. *Mineral. Mag.* **60**, 67-97.

DE GROOT, F.M.F., FIGUERIDO, M.O., BASTO, M.J., ABBATE, M., PETERSEN, H. & FUGGLE, J.C. (1992): 2p X-ray absorption of Ti in minerals. *Phys. Chem. Minerals* **19**, 140-147.

GUO, J. & GREEN, T.H. (1990): Experimental study of Ba partitioning between phlogopite and silicate liquid at upper-mantle pressure and temperature. *Lithos* **24**, 83-95.

HENDERSON, C.M.B., CHARNOCK, J.M., SMITH, J.V. & GREAVES, G.N. (1993): X-ray absorption spectroscopy of Fe, Mn, Zn, and Ti structural environments in staurolite. *Am. Mineral.* **78**, 477-485.

————, CRESSEY, G. & REDFERN, S.A.T. (1995): Geological applications of synchrotron radiation. *Radiat. Phys. Chem.* **45**, 459-481.

———— & GIBB, F.G.F. (1987): The petrology of the Lugar sill, S.W. Scotland. *Trans. R. Soc. Edinburgh, Earth Sci.* **77**, 325-347.

————, PENDLEBURY, K. & FOLAND, K.A. (1989): Mineralogy and petrology of the Red Hill alkaline igneous complex, New Hampshire, U.S.A. *J. Petrol.* **30**, 627-666.

KYSER, T.K. (1986): Stable isotope variations in the mantle. *Rev. Mineral.* **16**, 141-164.

VAN DER LAAN, G., PATTRICK, R.A.D., HENDERSON, C.M.B. & VAUGHAN, D.J. (1992): Oxidation state variations in copper minerals studied with Cu 2p X-ray absorption spectroscopy. *J. Phys. Chem. Solids* **53**, 1185-1190.

LEMARCHAND, F., VILLEMANT, B. & CALAS, G. (1987): Trace element distribution coefficients in alkaline series. *Geochim. Cosmochim. Acta* **51**, 1071-1081.

MANKSER, W.L., EWING, R.C. & KEIL, K. (1979): Barian–titanian biotites in nephelinites from Oahu, Hawaii. *Am. Mineral.* **64**, 156-159.

MITCHELL, R.H. (1981): Titaniferous phlogopites from the West Kimberley area, western Australia. *Contrib. Mineral. Petrol.* **76**, 243-251.

———— & PLATT, R.G. (1984): The Freeman's Cove volcanic suite: field relations, petrochemistry, and tectonic setting of nephelinite – basanite volcanism associated with rifting in the Canadian Arctic Archipelago. *Can. J. Earth Sci.* **21**, 428-436.

PARSONS, I. (1981): The Klokken gabbro–syenite complex, South Greenland: quantitative interpretation of mineral chemistry. *J. Petrol.* **22**, 233-260.

————, BROWN, W.L. & JACQUEMIN, H. (1986): Mineral chemistry and crystallization conditions of the Mboutou layered gabbro – syenite – granite complex, North Cameroon. *J. Petrol.* **27**, 1305-1329.

POWELL, R. & POWELL, M. (1974): Geothermometry and oxygen barometry using coexisting iron–titanium oxides: a reappraisal. *Mineral. Mag.* **41**, 257-263.

ROBERT, J.-L. (1976): Titanium solubility in synthetic phlogopite solid solutions. *Chem. Geol.* **17**, 213-227.

RYABCHIKOV, I.D. & GREEN, D.H. (1978): The role of carbon dioxide in the petrogenesis of highly potassic magmas. *Inst. Geol. Geofiz. Nauka, Novosibirsk* **403**, 49-64.

————, KOVALENKO, V.I., DIKOV, YU.P. & VLADYKIN, N.V. (1981): Titaniferous micas from the mantle: composition, structure, formation conditions, and possible role in the production of potassic alkaline magmas. *Geochim. Int.* **18**(3), 124-137.

SCHOFIELD, P.F., HENDERSON, C.M.B., CRESSEY, G. & VAN DER LAAN, G. (1992): 2p X-ray absorption spectroscopy in the Earth Sciences. *J. Synchrotron Rad.* **2**, 93-98.

SEIFERT, W. & KÄMPF, H. (1994): Ba-enrichment in phlogopite of a nephelinite from Bohemia. *Eur. J. Mineral.* **6**, 497-502.

SHAW, C.S.J. & PENCZAK, R.S. (1996): Barium- and titanium-rich biotite and phlogopite from the Western and Eastern Gabbro, Coldwell alkaline complex, northwestern Ontario. *Can. Mineral.* **34**, 967-975.

SOLIE, D.N. & SU, SHU-CHUN (1987): An occurrence of Ba-rich micas from the Alaska Range. *Am. Mineral.* **72**, 995-999.

THOMPSON, R.N. (1977): Primary basalts and magma genesis. III. Alban Hills. Roman comagmatic province, central Italy. *Contrib. Mineral. Petrol.* **60**, 91-108.

TRACY, R.J. (1991): Ba-rich micas from the Franklin Marble, Lime Crest and Sterling Hill, New Jersey. *Am. Mineral.* **76**, 1683-1693.

TRØNNES, R.G., EDGAR, A.D. & ARIMA, A. (1985): A high-pressure - high temperature study of TiO₂ solubility in Mg-rich phlogopite: implications to phlogopite chemistry. *Geochim. Cosmochim. Acta* **49**, 2323-2329.

WADSWORTH, W.J. (1988): Silicate mineralogy of the Middle Zone cumulates and associated gabbroic rocks from the Insch intrusion, N.E. Scotland. *Mineral. Mag.* **52**, 309-322.

WAGNER, C. & VELDE, D. (1986): The mineralogy of K-richterite-bearing lamproites. *Am. Mineral.* **71**, 17-37.

WAYCHUNAS, G.A. (1987): Synchrotron radiation XANES spectroscopy of Ti in minerals: effects of Ti bonding distances, Ti valence, and site geometry on absorption edge structure. *Am. Mineral.* **72**, 89-101.

————, APTED, M.J. & BROWN, G.E., JR. (1983): X-ray K-edge absorption spectra of Fe minerals and model compounds: near edge structure. *Phys. Chem. Minerals* **10**, 1-9.

WENDLANDT, R.F. (1977): Barium-phlogopite from Haystack Butte, Highwood Mountains, Montana. *Carnegie Inst. Wash., Year Book* **76**, 534-539.

WILSON, J.R. & LARSEN, S.B. (1985): Two-dimensional study of a layered intrusion – the Hyllingen Series, Norway. *Geol. Mag.* **122**, 97-124.

YAU, YU-CHYI, PEACOR, D.R. & ESSENE, E.J. (1986): Elemental normalizations and substitution mechanisms of titanium in phlogopite. *Eos, Trans Am. Geophys. Union* **67**, 415 (abstr.).

ZHANG, MING, SUDDABY, P., THOMPSON, R.N. & DUNGAN, M.A. (1993): Barian–titanian phlogopite from potassic lavas in northeast China: chemistry, substitutions and paragenesis. *Am. Mineral.* **78**, 1056-1065.